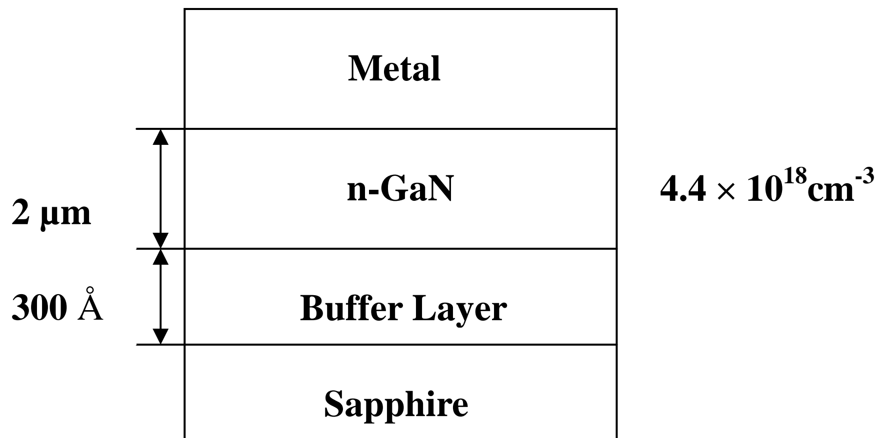

(a) Structure of metal/n-GaN contact.

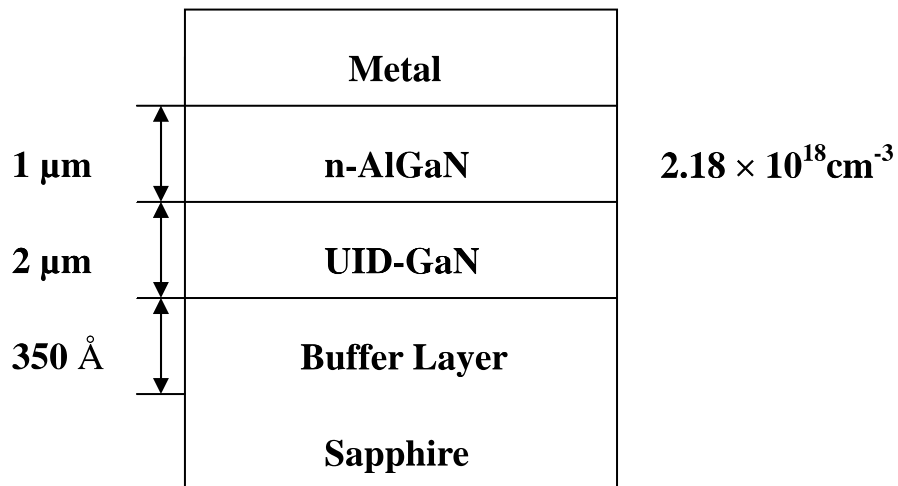

(b) Structure of metal/n-AlGaN contact.

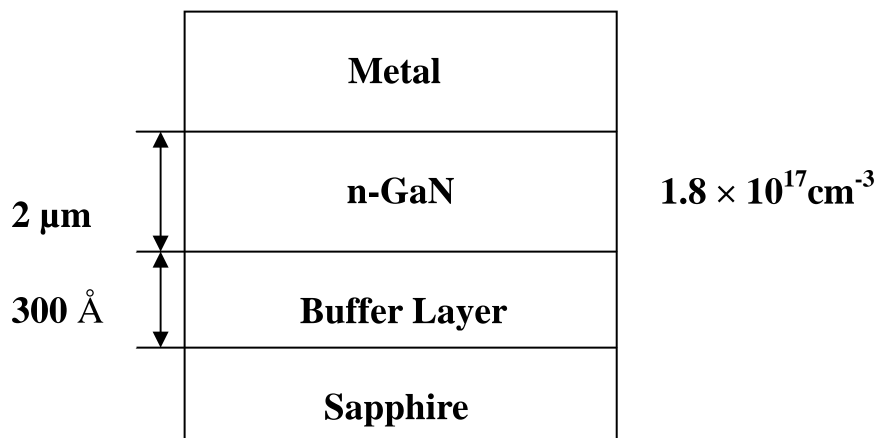

(c) Structure of metal/n-GaN contact.

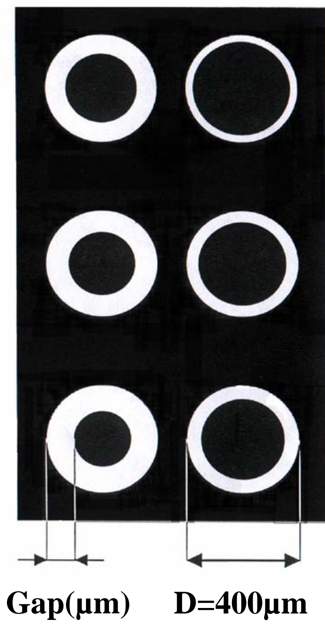

Gap(μm)	Correction factor
5	1.013
10	1.026
15	1.040
25	1.070
35	1.103
45	1.139

(a)

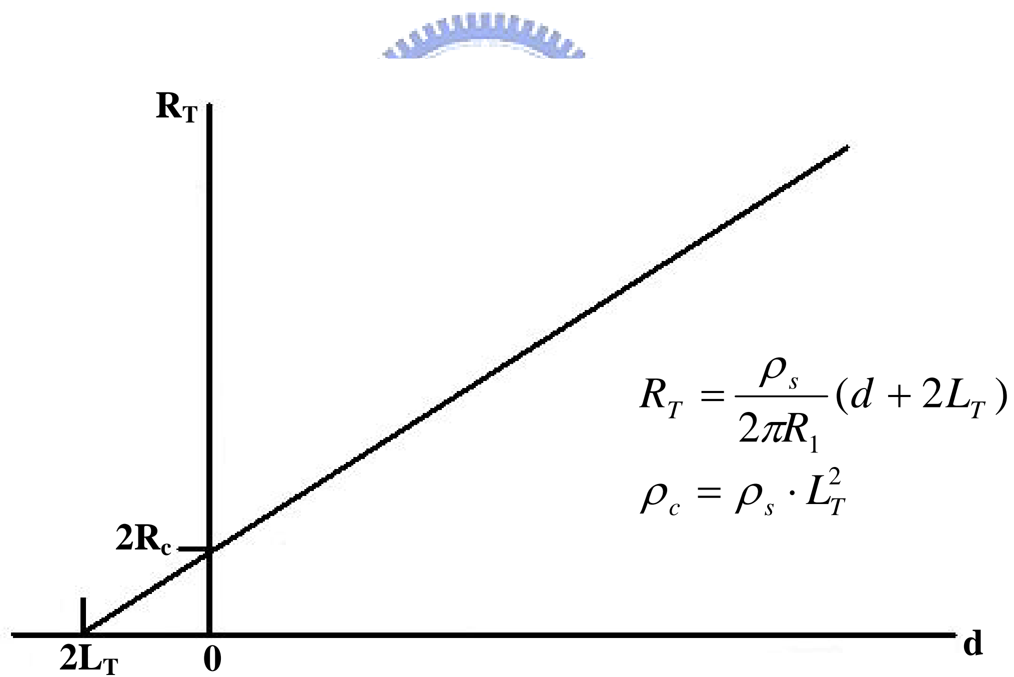

(b)

Figure 4-2. (a) CTLM pad structure and correction factor; (b) The plotting of total resistance against gap distance.

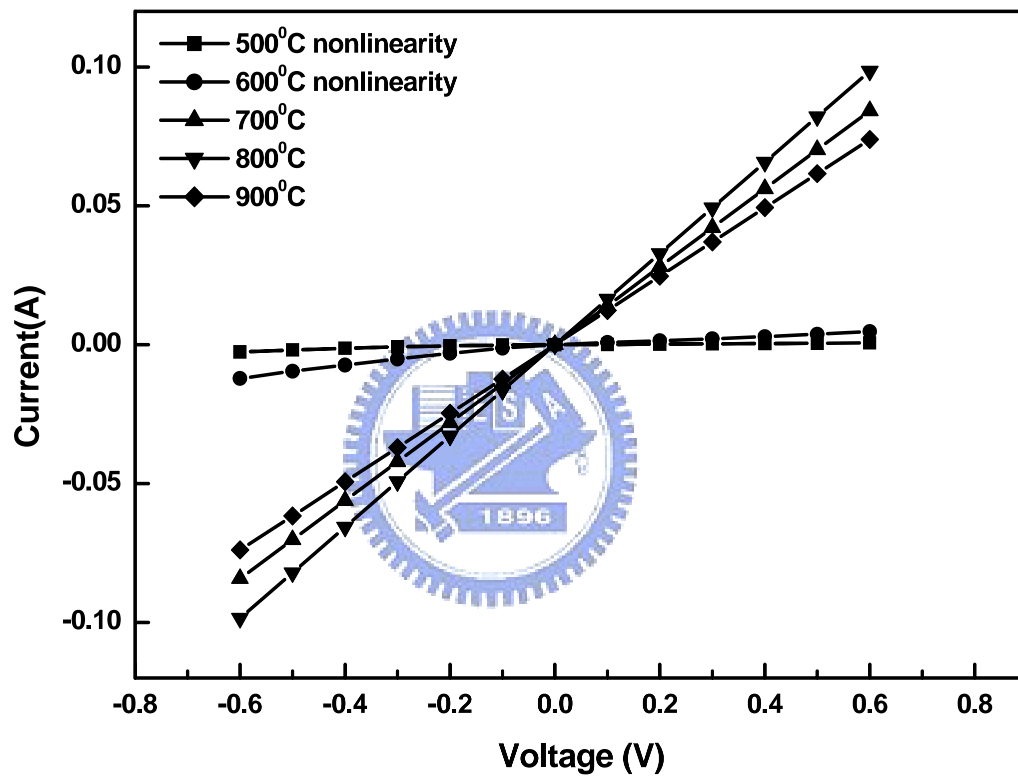

Figure 4-3. The I-V curves measured for Ti/Al/Ni/Au contact on n-GaN annealed at different conditions (Diode gap 10 μm).

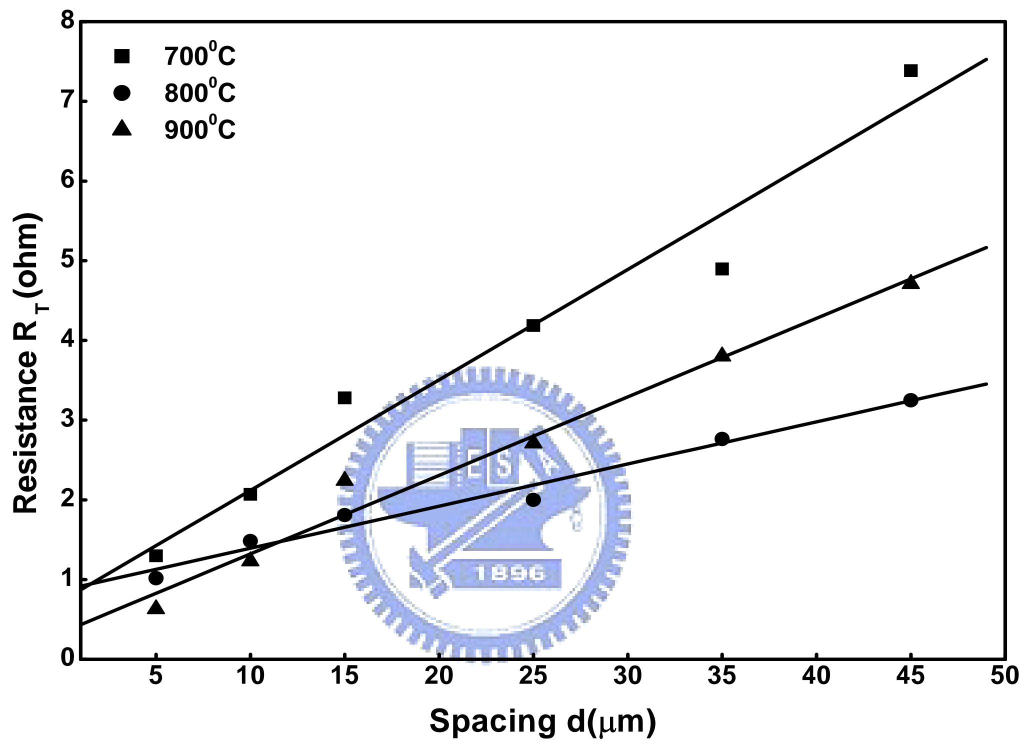

Figure 4-4. Total resistance (***R_T***) *v.s.* gap spacing at different annealing temperatures for Ti/Al/Ni/Au contact on n-GaN.

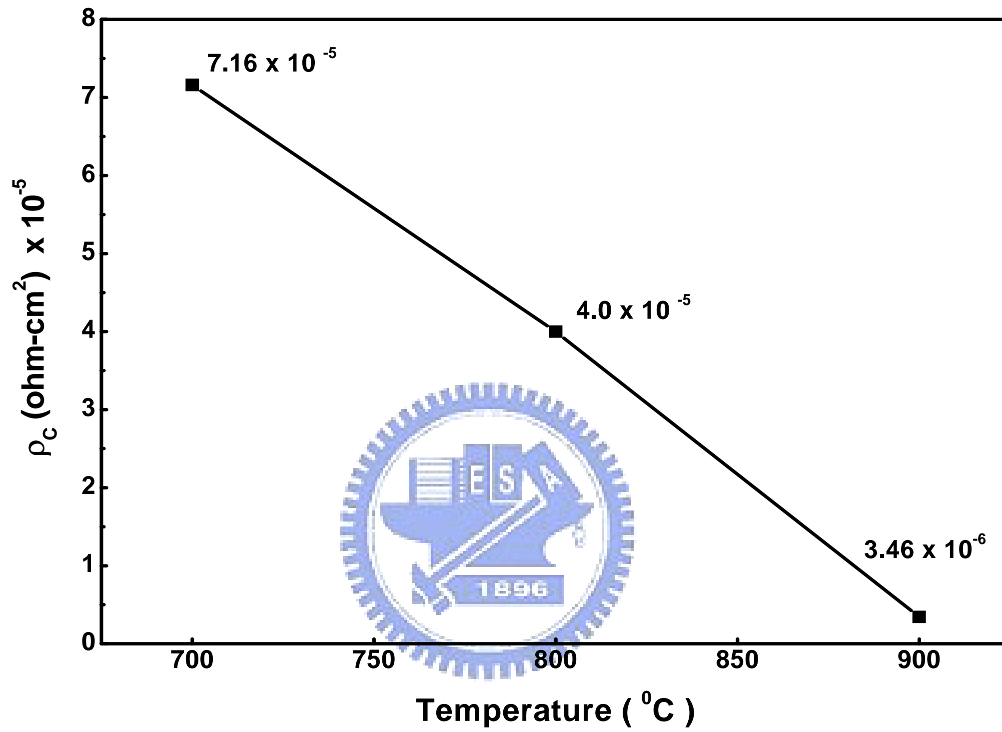

Figure 4-5. Specific contact resistivity as a function of annealing temperature for Ti/Al/Ni/Au contact on n-GaN.

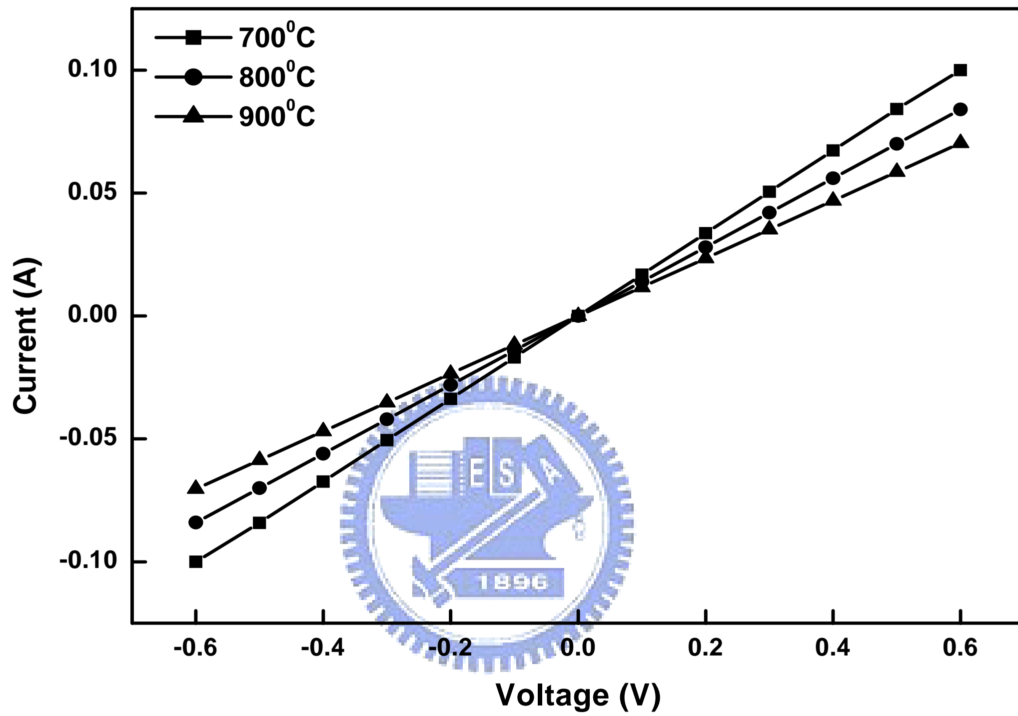

Figure 4-6. The I-V curves measured for Ti/Al/Ni/Au contact on n-AlGaN annealed at different conditions (Diode gap 10 μm).

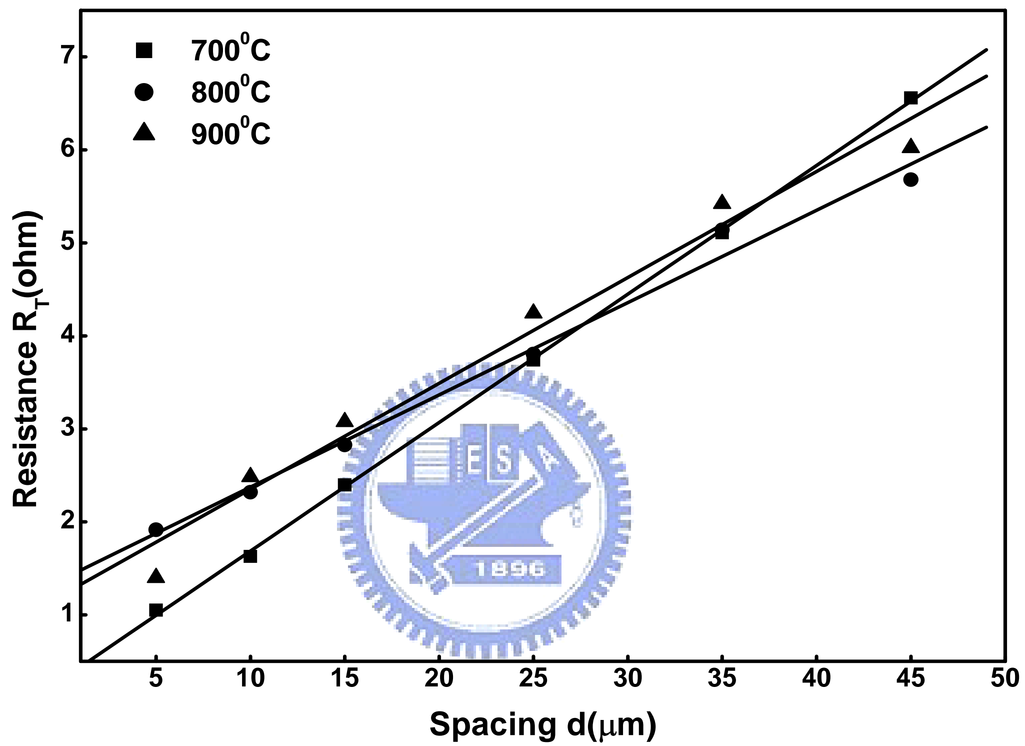

Figure 4-7. Total resistance *v.s.* gap spacing at different annealing temperatures for Ti/Al/Ni/Au contact on n-AlGaN.

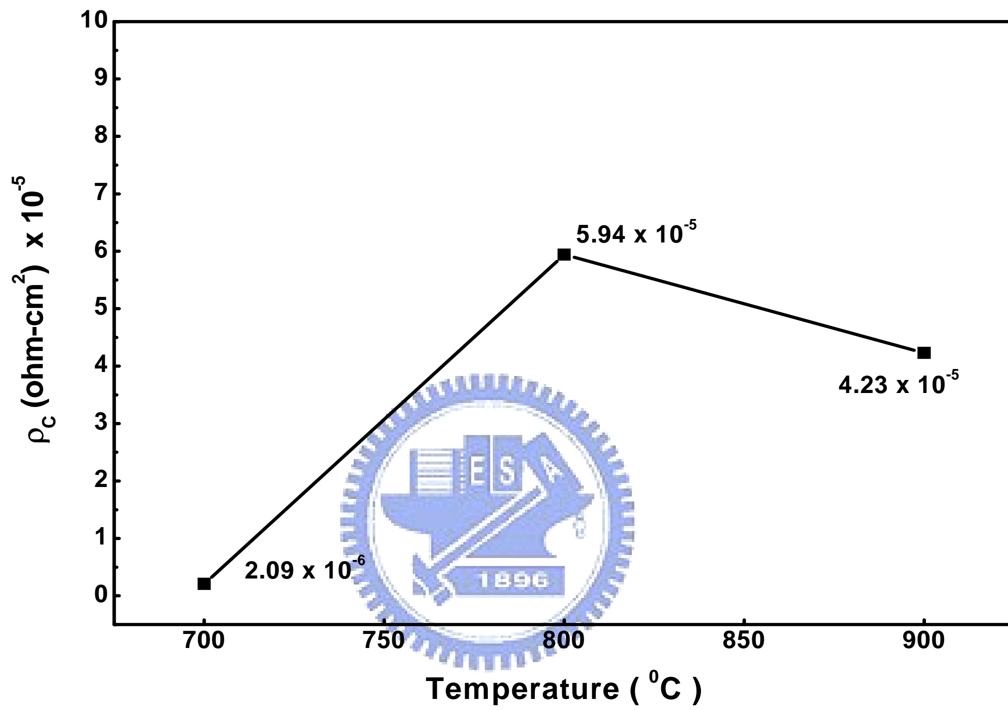

Figure 4-8. Specific contact resistivity as a function of annealing temperature for Ti/Al/Ni/Au contact on n-AlGaN.

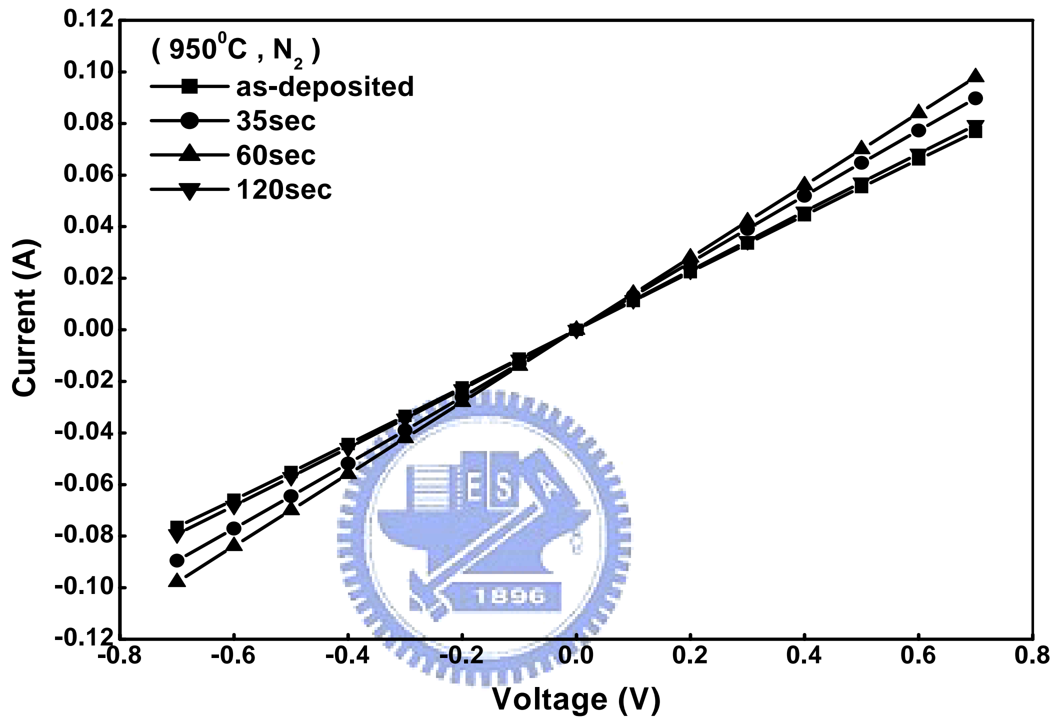

Figure 4-9. The I-V curves measured for Ti/Al/Pt/Au contact on n-AlGaN annealed at different conditions (Diode gap 10 μm).

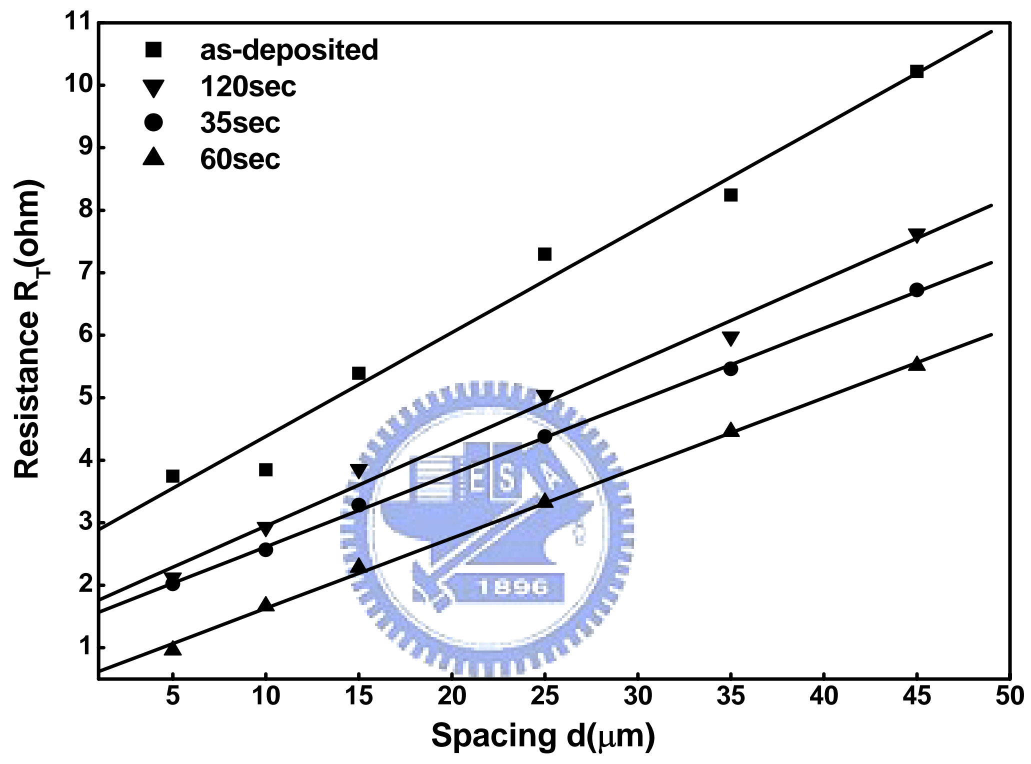

Figure 4-10. Total resistance *v.s.* gap spacing at different annealing times for Ti/Al/Pt/Au contact on n-AlGaN

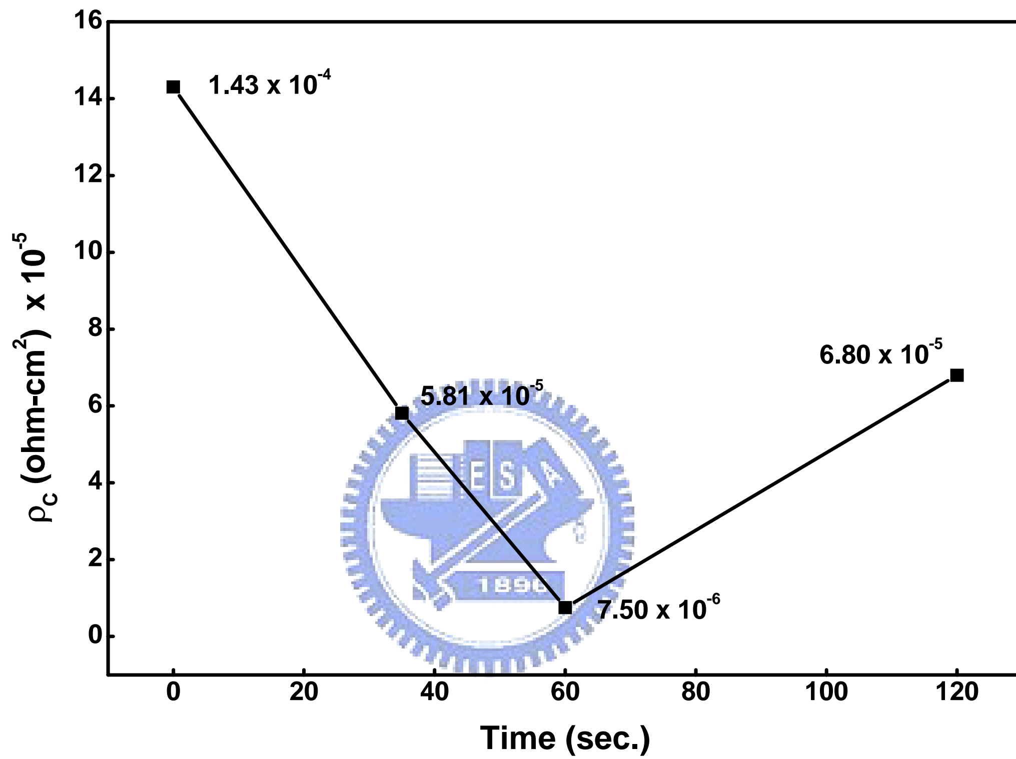

Figure 4-11. Specific contact resistivity as a function of annealing time for Ti/Al/Pt/Au contact on n-AlGaN.

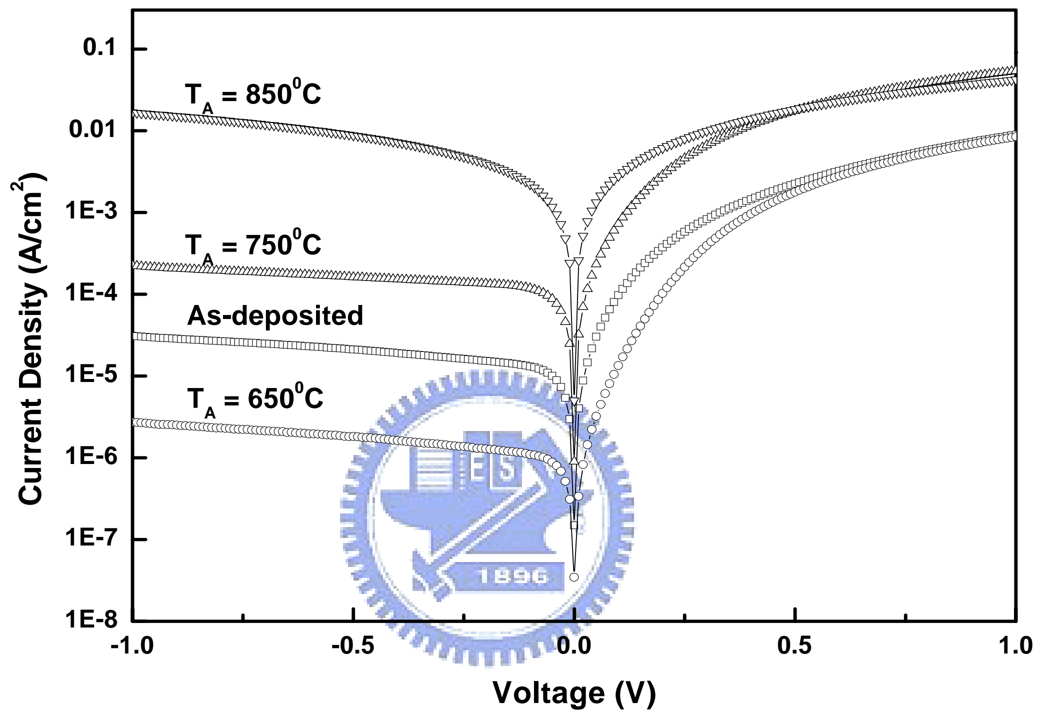

Figure 4-12. Current *v.s.* applied voltage for $TiWN_x$/n-GaN; (b) WN_x/n-GaN.

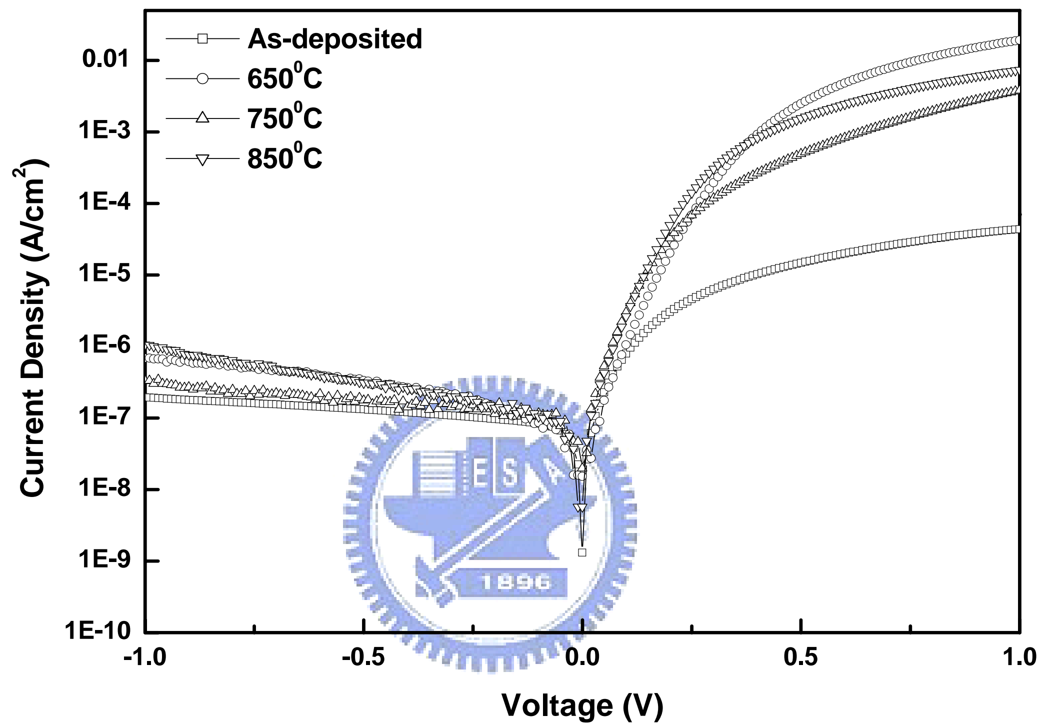

Figure 4-13. Current *v.s.* applied voltage for WN_x/n-GaN.

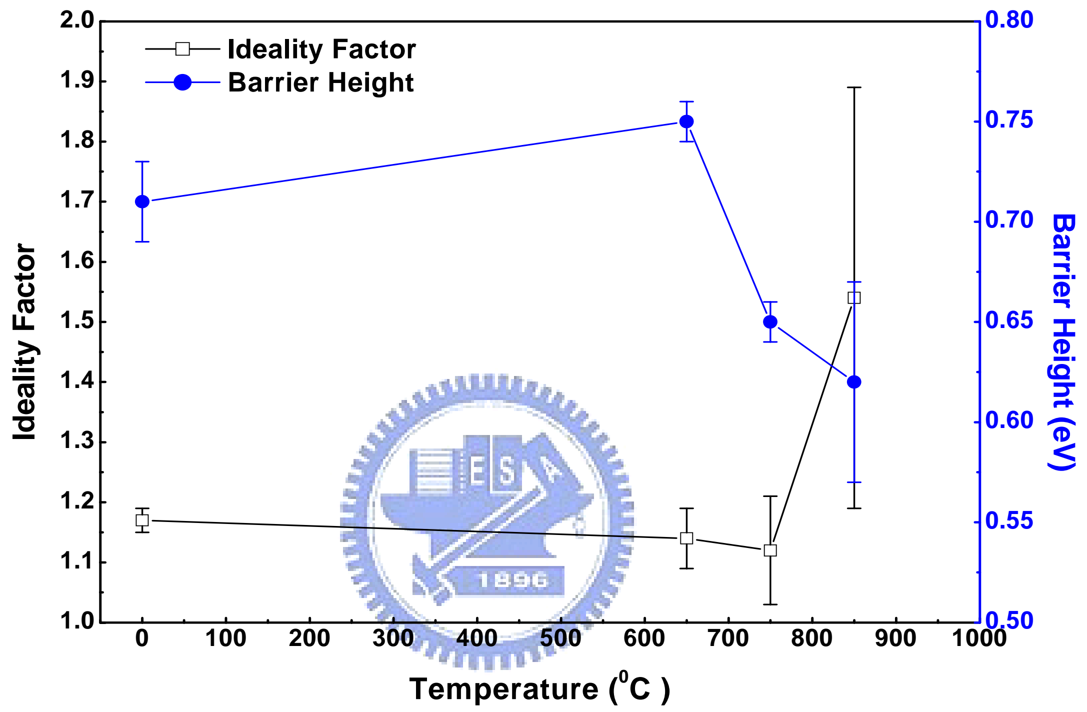

Figure 4-14. Schottky barrier height and ideality factor *v.s.* annealing temperature for $TiWN_x$/n-GaN

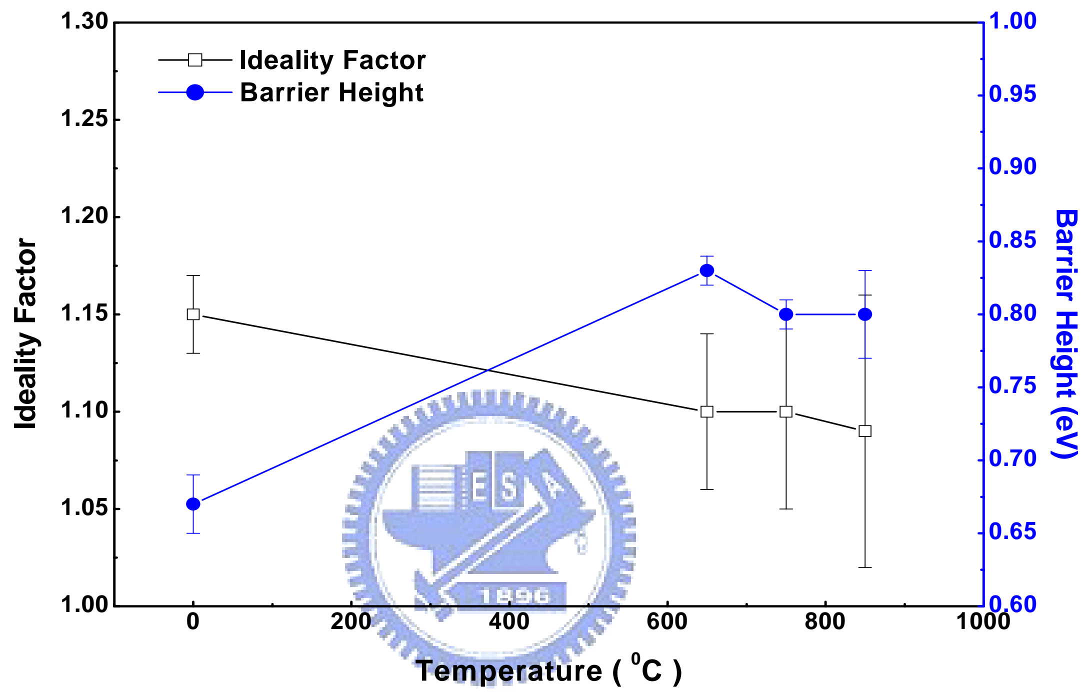

Figure 4-15. Schottky barrier height and ideality factor *v.s.* annealing temperature for WN_x/ n-GaN.

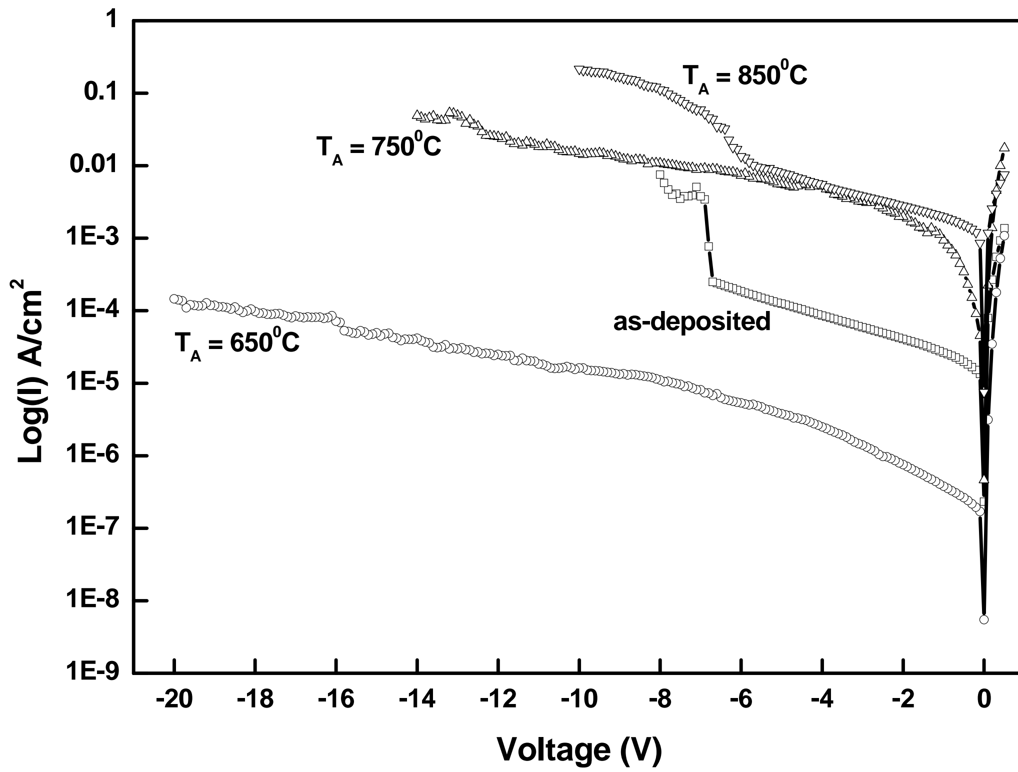

Figure 4-16. Leakage current density *v.s.* applied voltage of $TiWN_x$/n-GaN.

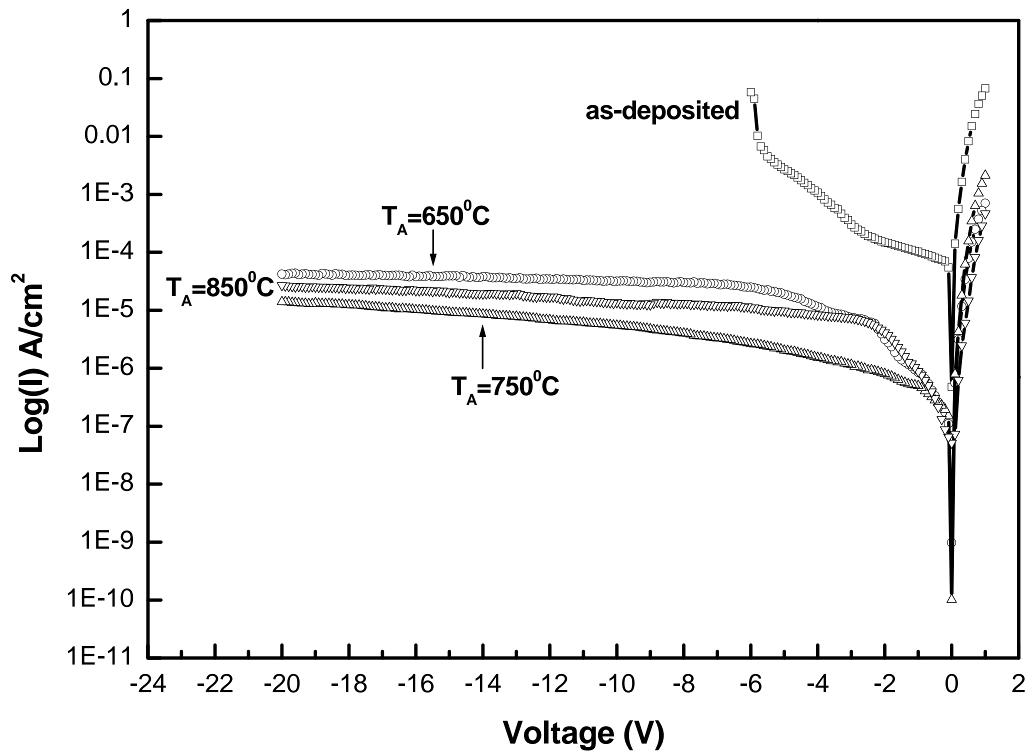

Figure 4-17. Leakage current density *v.s.* applied voltage of WN_x/n-GaN.

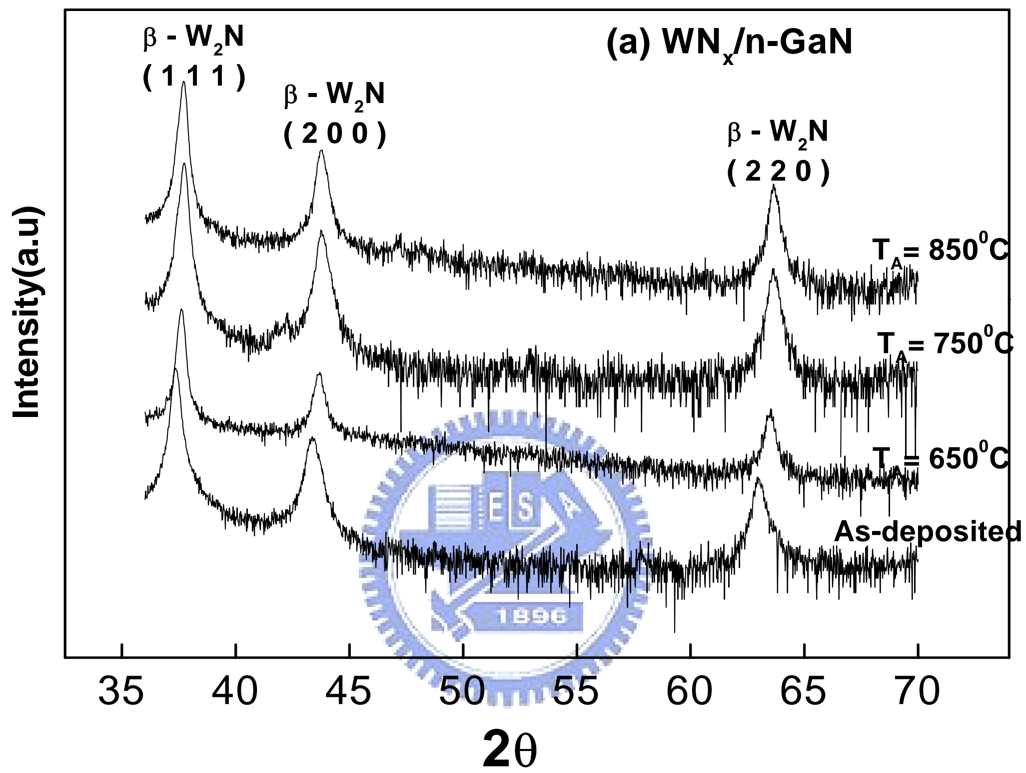

Figure 4-18. The XRD spectra of WN_x/n-GaN contacts at different annealing temperatures.

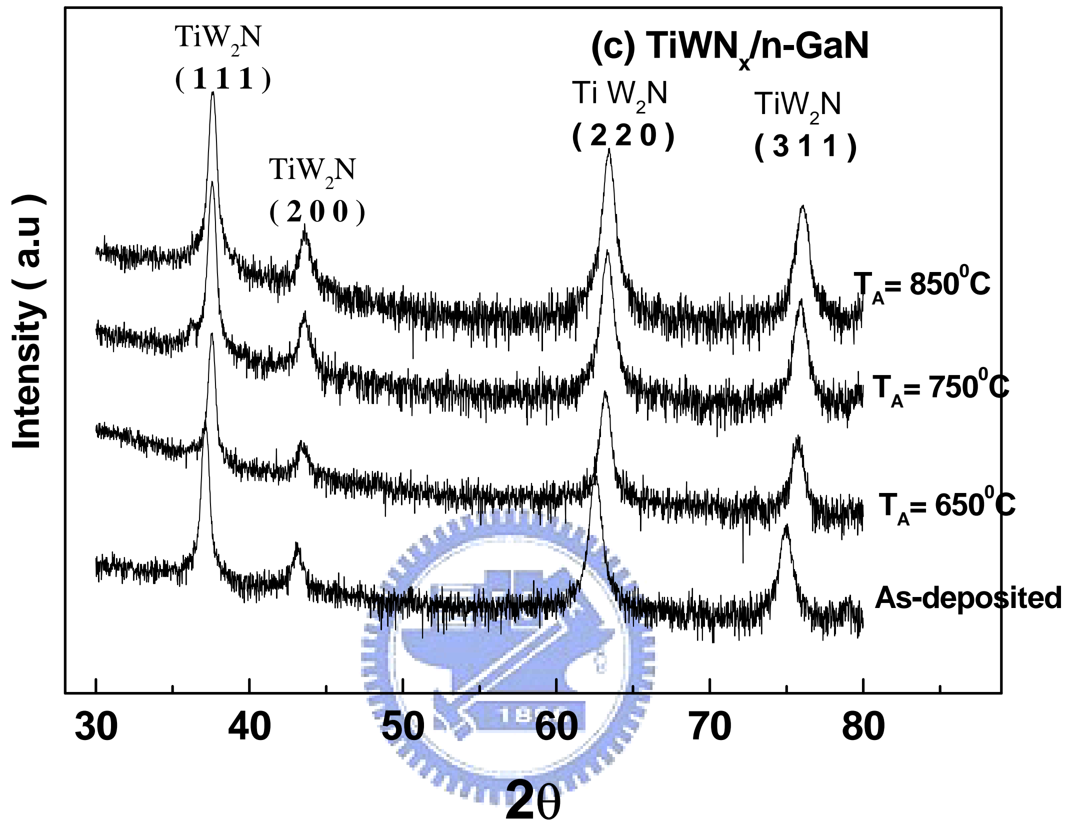

Figure 4-19. The XRD spectra of the $TiWN_x$/n-GaN contacts after different annealing temperatures.

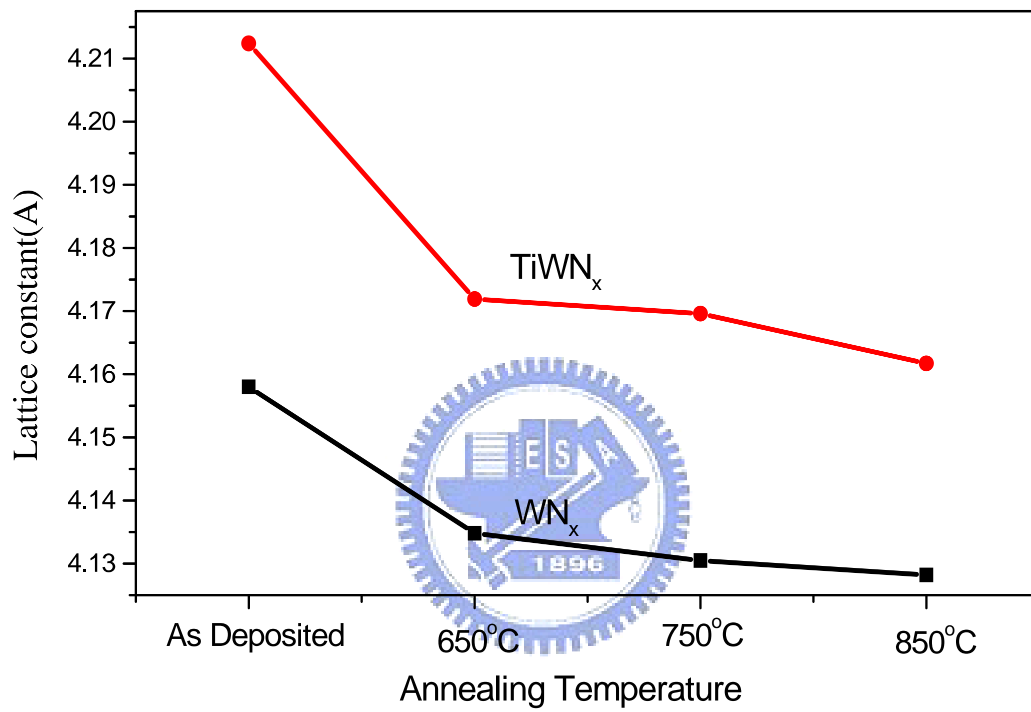

Figure 4-20. Lattice constant of WN_x and $TiWN_x$ before and after annealing.

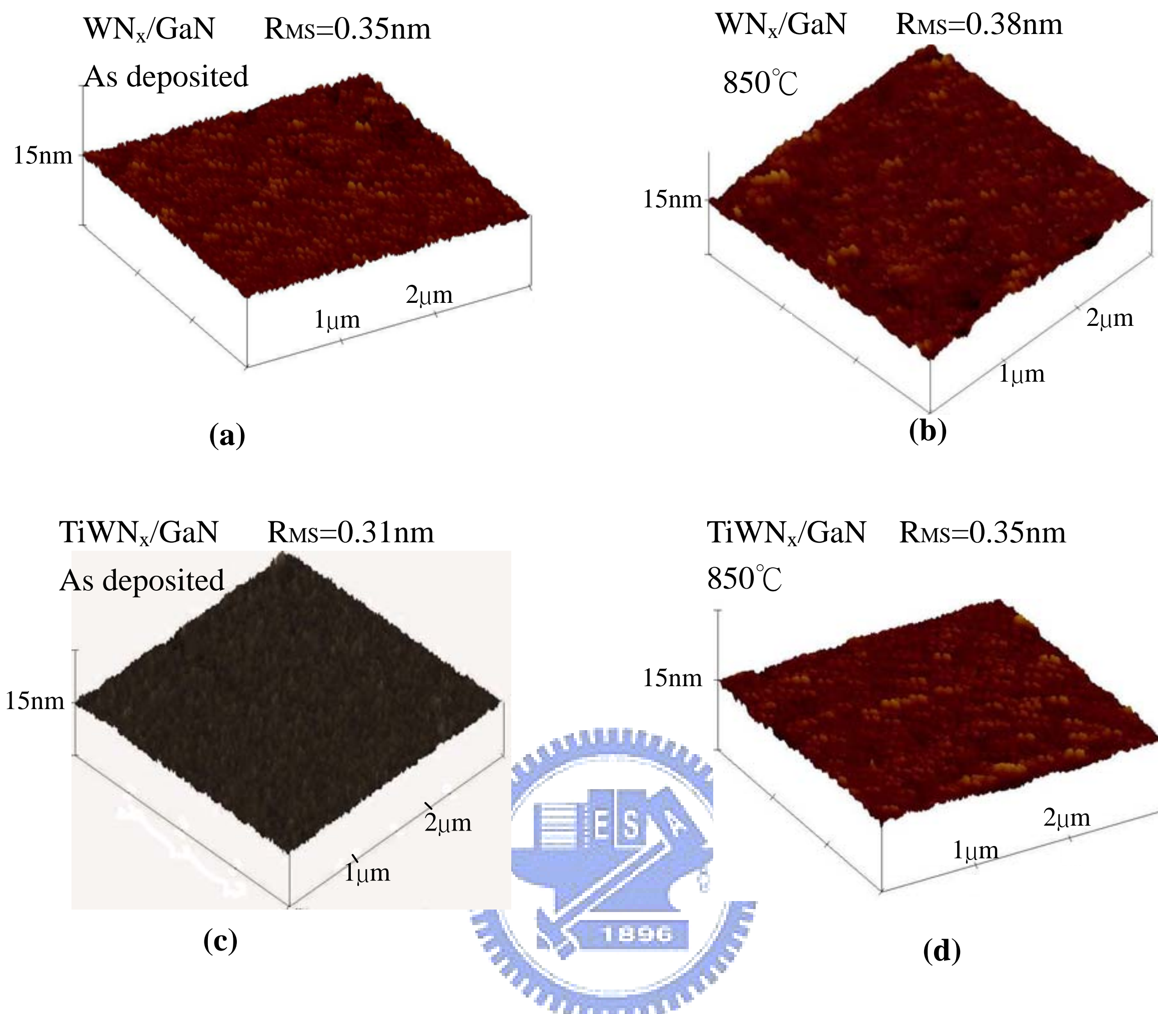

Figure 4-21. Surface morphology analysis by AFM for (a) As-deposited WN_x film. (b) WN_x film after annealing at 850℃. (c) As-deposited $TiWN_x$ film. (c) $TiWN_x$ film after annealing at 850℃.

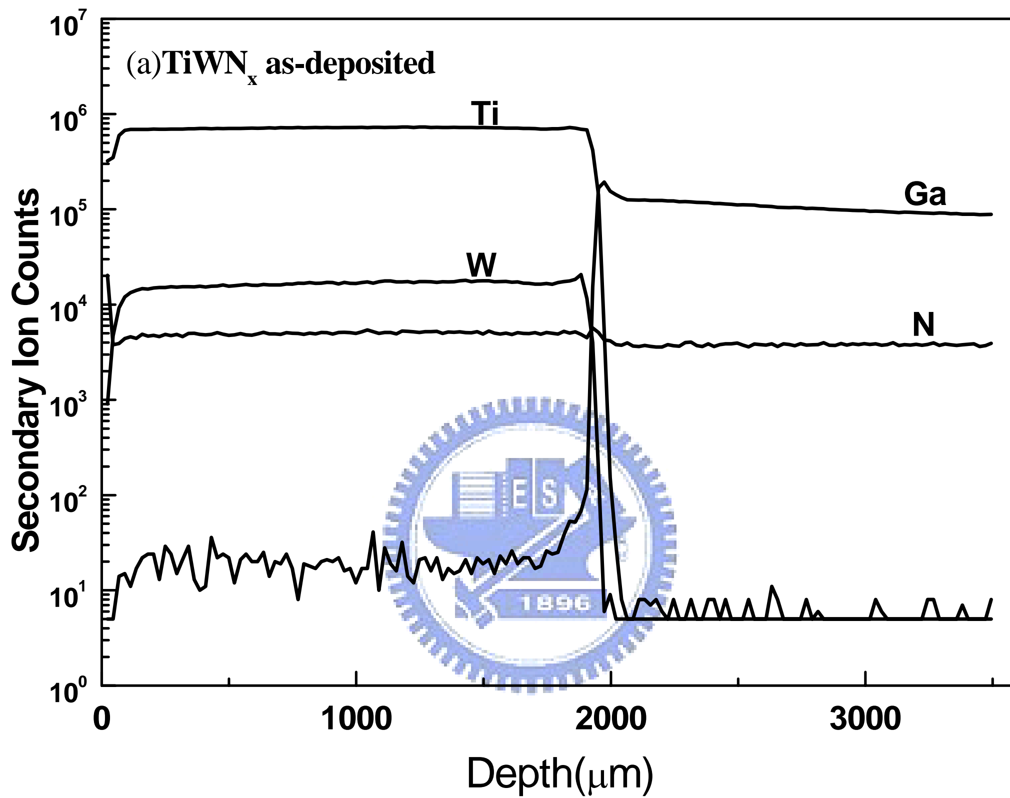

Figure 4-22. SIMS depth profiles of the TiWN$_x$/n-GaN contacts after thermal treatments (a)As-deposited；(b)After 650℃ annealing; and (c) After 850℃ annealing.

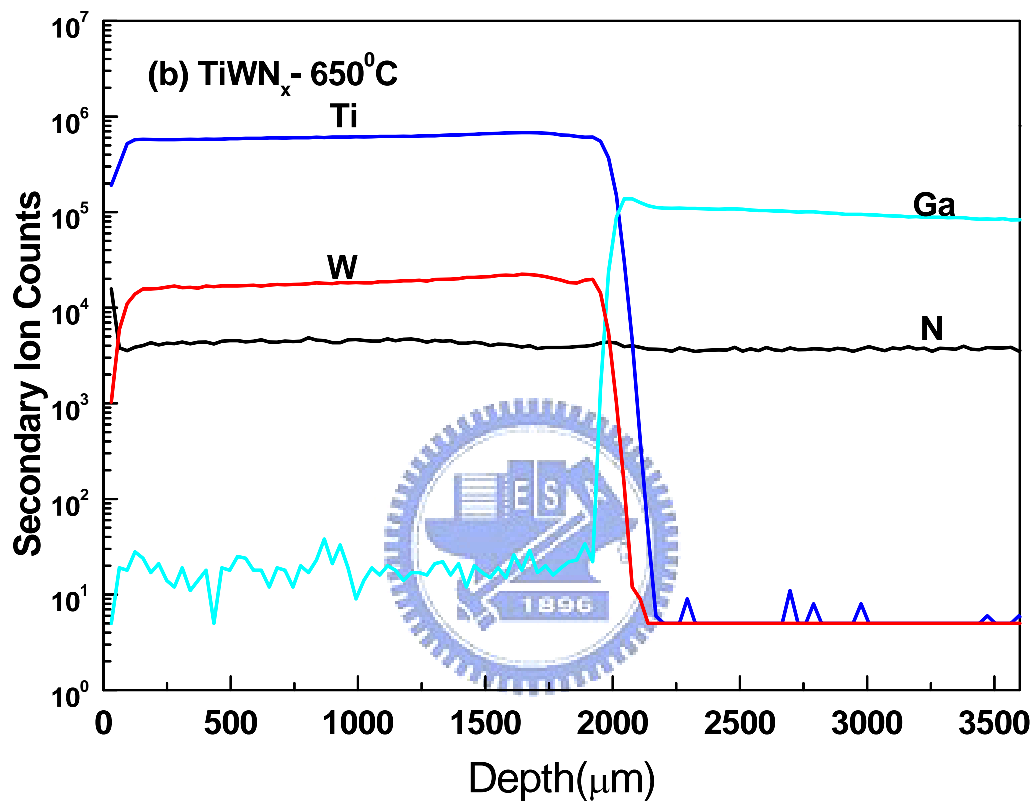
(b) $TiWN_x$- 650^0C
Ti
Ga
W
N
Secondary Ion Counts
10^0
10^1
10^2
10^3
10^4
10^5
10^6
10^7
0
500
1000
1500
2000
2500
3000
3500
Depth(μm)
1896

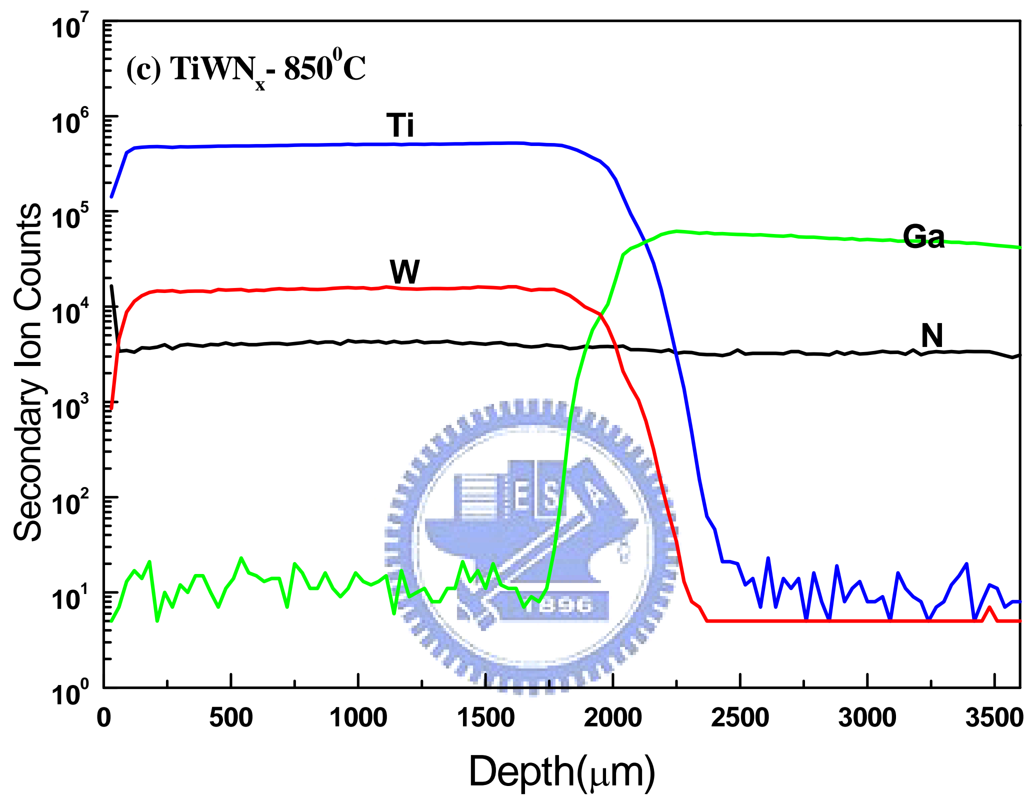
(c) TiWN$_x$- 850^{0}C
Ti
W
Ga
N
Secondary Ion Counts
Depth(μm)
10^0
10^1
10^2
10^3
10^4
10^5
10^6
10^7
0
500
1000
1500
2000
2500
3000
3500

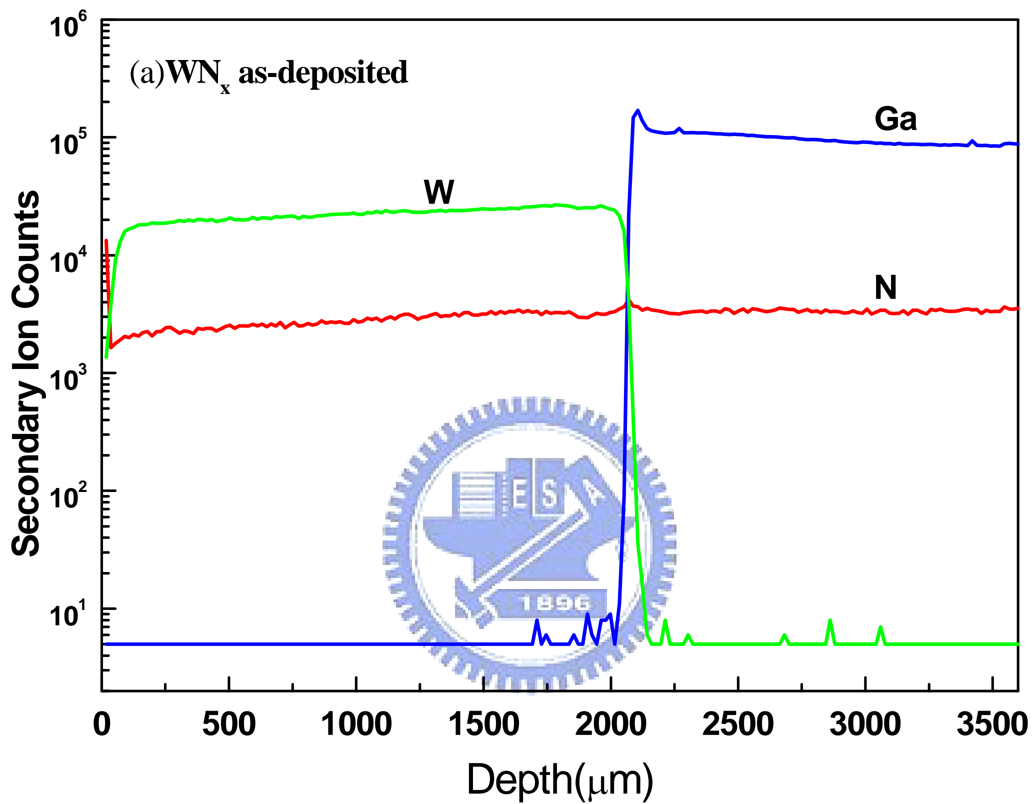

(a)

Figure 4-23. SIMS depth profiles of the WN_x/n-GaN contacts after thermal treatments (a)As-deposited；(b)After 650℃ annealing;(c) After 850℃ annealing.

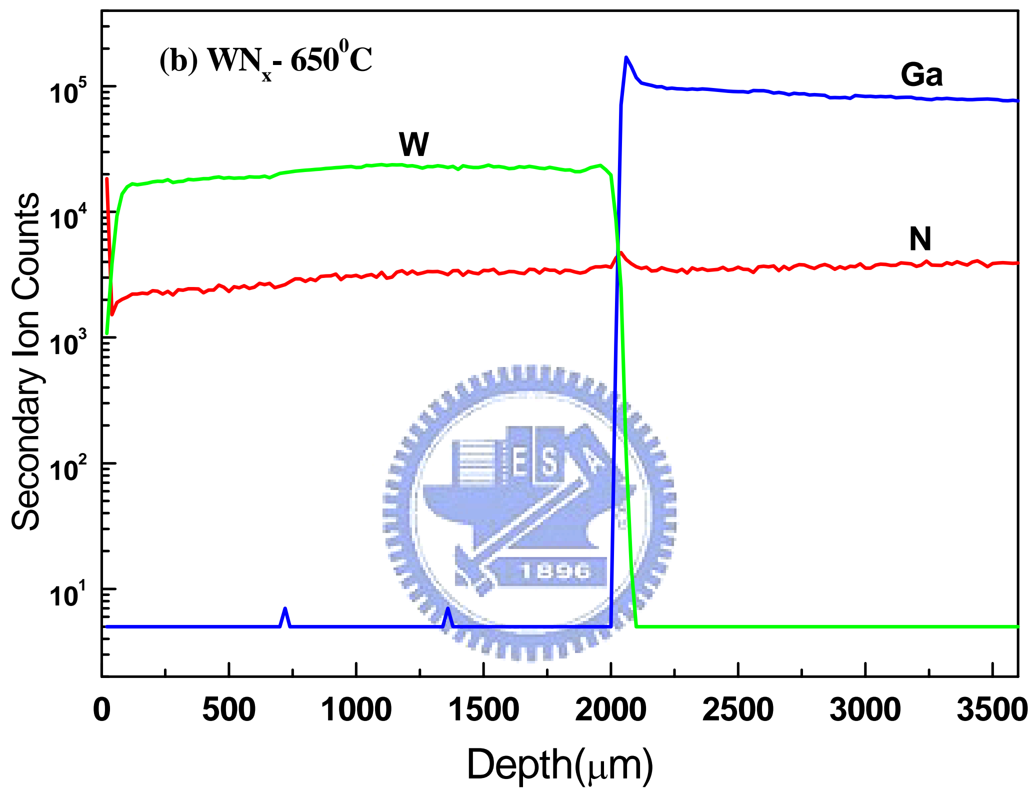

(b)

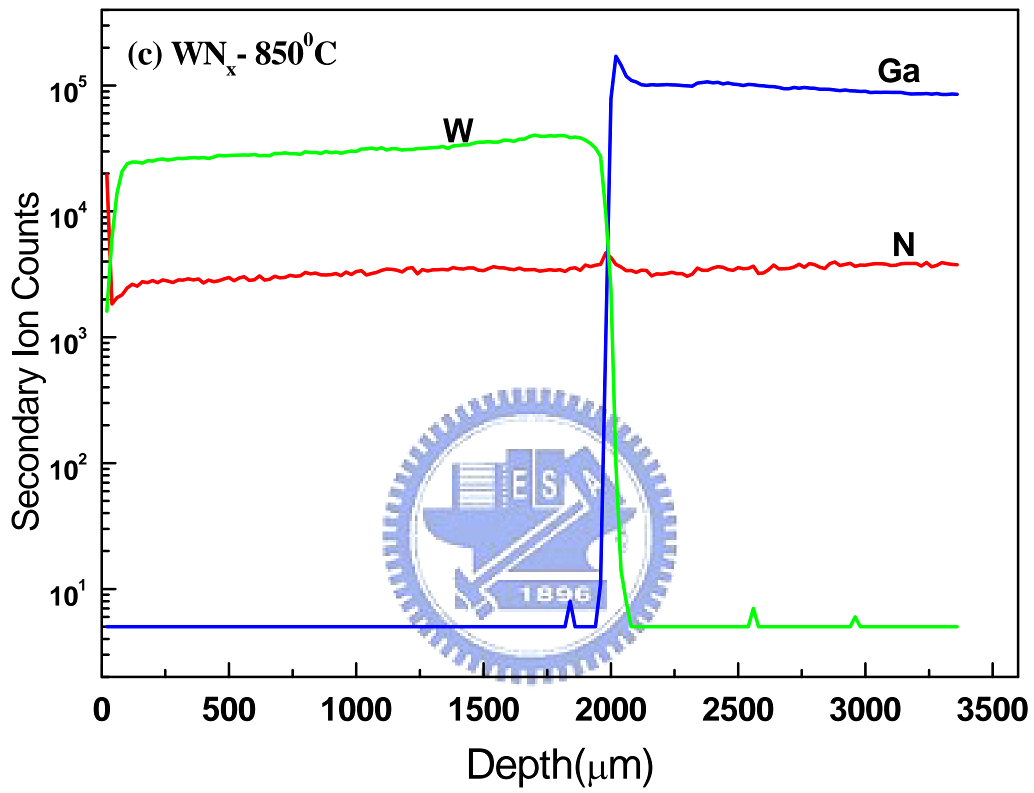

(c)